Laser photoluminescence spectrometer based on charge-coupled device detection for silicon-based photonics

O. H. Y. Zalloum, M. Flynn, T. Roschuk, J. Wojcik, E. Irving, and P. Mascher
Centre for Emerging Device Technologies and Department of Engineering Physics, McMaster University, Hamilton, Ontario L8S 4L7, Canada

(Received 16 September 2005; accepted 12 January 2006; published online 24 February 2006)

We describe and characterize a multichannel modular room temperature photoluminescence spectroscopy system. This low cost instrument offers minimization of size and complexity as well as good flexibility and acceptable spectral resolution. The system employs an efficient flexible front end optics and a sensitive spectrometer with a charge-coupled device array detector. The spectrometer has no moving parts and is more robust than a scanning system. The scientific motivation was to enable the photoluminescence study of various silicon photonics structures. Typical applications are presented for SiO_x $(x<2)$ films. It is demonstrated that high-quality steady state photoluminescence data with excellent signal to noise enhancement capability can be delivered besides the ability to perform simultaneous multiwavelength measurements in one shot. This instrument is shown to be useful for evaluating semiconductor wafers, including those intended for light emitting structures from silicon-based photonic crystals. The design, construction, calibration, and the unique features of this system are presented, and performance tests of a prototype are discussed. © *2006 American Institute of Physics.* [DOI: 10.1063/1.2173030]

I. INTRODUCTION

Photoluminescence (PL) spectroscopy is a widely used technique for the study of semiconductor materials.[1] The PL response can be used to study the recombination mechanisms,[2,3] peak emission wavelengths, and quantum efficiencies that may be expected from light emitting structures produced from a given wafer. PL analysis can also be applied to study passivation,[4] impurity levels, and defect detection,[5,6] the effects of wafer processing and growth procedures[7] and post-treatment parameters[8] on a material's luminescence properties, and to assess the potential of a material before the final fabrication into light emitting structures.[9] Because lasers are monochromatic, intense, and readily focused, they are the instruments of choice for direct photoluminescence excitation.

Under conventional PL techniques, a scanning stage monochromator equipped with a photomultiplier tube (PMT) or single element detector is used for analyzing the emission from a sample.[10,11] The disadvantage of this technique is that a considerable amount of time may be required to collect a single spectrum. With an array detector, mounted onto an imaging spectrometer, however, substantial spectral information can be measured rapidly and simultaneously. A variety of multichannel detectors were provided, initially with a silicon intensified target (SIT) vidicon detectors[12] and photodiode array detectors[13] (PDA) or more recently with charge-coupled device (CCD) arrays.

Novel components, such as flexible fiber optic inputs, flat field internal optical components, and sensitive CCDs, have greatly improved the versatility of modern PL instruments. When these novel components are combined they form the basis of new generation fiber optic spectrometer systems, which can be read out and controlled by fast analog to digital (A/D) converters mounted in powerful, portable computer systems.[14] Fourier transform spectrometers have also been applied to photoluminescence measurements.[15]

In this article, we present and carefully characterize a simple, modular, inexpensive but efficient, macro-PL system based on the CCD detection for silicon-based photonics. The characterization is important in order to evidence the peculiarities of this technique and to allow its use at the best of its capabilities. This system is optimized for the visible spectrum. It makes use of an Ocean Optics S2000 spectrometer (Ocean Optics Inc., Dunedin, FL). The modular simple design allows for flexibility and is pedagogically valuable. We review in detail the design and calibration for this application. The importance of correction for the instrument response function is also highlighted which is often overlooked.

II. DESIGN CONSIDERATIONS

The choice of excitation source is critical in any PL measurement. For efficient optical excitation of electron-hole pairs, the laser energy must be greater than the band gap of the semiconductor under study. The intensity of the incident light controls the density of photoexcited electrons and holes; a critical property of the PL experiment. When the carrier density is low, the measurement is dominated by the discrete defect and impurity sites at the interfaces and within the bulk of the material.[1] An intense excitation source and a sensitive detector are required to obtain the adequate signal to noise ratio (SNR) that is necessary for the generation of good quality PL spectra. The Si-based nanocrystallites can exhibit visible PL although bulk silicon has a relatively small

(1.11 eV at room temperature) and indirect band gap. A 325 nm (3.82 eV) He–Cd laser (Kimmon Electric Co., Ltd) is used as a pump source in the instrument described herein.

Other design considerations arise from the choice of spectral and spatial resolutions and from the minimum detectable signal that is required to produce a high-quality PL spectrum within a practical integration interval. The spectrometer used in this study uses an effective 2048 element linear CCD array including a number of blackened pixels. Data are transferred to a computer through a linear 12 bit A/D card (ADC1000-USB). The linear A/D converter quantifies the number of measured electrons to corresponding digital levels of detected signal (counts). The grating has 600 lines/mm and is configured to provide a large spectral window (~650 nm: ~350–1000 nm). The optical resolution, measured as full width at half maximum (FWHM), of a monochromatic source depends on the groove density (lines/mm) of the grating and the diameter of the entrance optics (optical fiber or slit in our case). The resolution increases with an increase in the groove density of the grating, but at the expense of spectral range and signal strength. In addition, the resolution increases as the slit width decreases, but at the expense of signal strength.[16] Thus, it is a combination of the linear dispersion of the grating and the lateral dimension of the input slit and the detector array elements that ultimately determines the spectral resolution of a PL measurement.

The FWHM resolution of the fiber optic spectrometer S2000 was limited in our case by the effective width of the light beam from the entrance slit. We used a 50 μm slit which results in a Gaussian response function with a FWHM of 2.1 nm.

Only part of the luminescence from the sample can be collected due to the coupling, transmission, and reflection losses and the finite size of the optics. The collection efficiency is of crucial importance, especially in the cases of low intensity excitation or low PL signal levels. The geometric etendue,[17] G, characterizes the ability of an optical system to accept light. It is a function of the area, S, of the emitting source, and the solid angle, Ω, into which it propagates. The etendue therefore, is a limiting function of system throughput.

$$G = \int \int dS d\Omega. \tag{1}$$

Following integration for a conical beam the axis of which is normal to source of area S,

$$G = S\Omega = \pi S \sin^2 \theta_{1/2} = \pi S(\mathrm{NA})^2, \tag{2}$$

where $\theta_{1/2}$ is the half angle in air relative to the source axis, and NA is the numerical aperture.

Applied to the described spectrometer, S in Eq. (2) is the usable area of the slit and Ω is the solid angle of the cone of acceptance of the spectrometer. The NA of the fiber matches that of the spectrometer and the usable area of the slit is smaller than the core area of the fiber optic. The etendue, therefore, is a constant of the system and is limited by the spectrometer entrance slit. The spectrometer has $50\times \sim 1000$ μm^2 (factory installed) input slit mounted at the input focal plane, against which the input fiber (core diameter 600 μm) is butt coupled. The large core diameter would effectively enhance the signal with no loss of resolution. Larger core diameters may not be very useful because the linear CCD detector cannot efficiently collect the light from the entire height of the slit. The portion of PL flux lost in traversing the collection and detection path including those losses at the fiber-slit interface can be accounted for by the intensity calibration of the system as described in Sec. IV B below.

Noise sources for a CCD pixel are well documented and well understood.[18] Thus a detailed discussion of this point is omitted. A PL measurement is based ultimately on counting photons, and is governed by Poisson statistics.[19] In this work, signal to noise enhancement of the PL spectra is accomplished by the use of a combination of extended integration times (typically 2500 ms), dark current subtraction, and scan averaging so that the dynamic range of the individual spectra can be improved significantly. The fixed pattern CCD noise is highly repeatable and can be almost completely eliminated by subtracting a dark acquisition of the same integration time and smoothing size interval as that of the illuminated sample of interest. Dark acquisition is accomplished by blocking the laser output using a factory installed mechanical shutter. Therefore, there is a little penalty in using the speed advantage of the CCD array in taking multiple spectra in order to improve the signal to noise ratio under low-light-level conditions. The signal to noise ratio of the resultant averaged spectrum is improved over a single pixel in a single scan by a factor of $\sqrt{nb}$, where $n \geqslant 1$ is the number of spectra that are acquired and averaged, and b is the total number of spectral points binned in boxcar smoothing. It will be noted that in boxcar smoothing, the signal at each wavelength is averaged with the signal at one or more wavelengths on either side. A value of n_b averages n_b points to the right and n_b points to the left. Thus the SNR improves by $\sqrt{b}$,[18–20] where $b = 2n_b + 1$ and $n_b \geqslant 0$. Typically, we used $n_b = 2$ to maintain $b \leqslant$ the resulting resolution in pixels (=6.5 pixels). The method of averaging also minimizes the need for device cooling to reduce the dark current noise.

III. DESCRIPTION OF THE PL SYSTEM

A. General layout

The experimental layout is shown in Fig. 1. The beam from a 325 nm He–Cd laser is passed through an iris diaphragm (1/2 in. aperture) into the sample without focusing. The sampled area equals the area defined by the image of the receiving fiber core on the exit surface of the sample. Ideally, the core's image of the receiving fiber must be aligned with the center of the projection of laser beam cross section along the sample exit surface observed by the spectrometer. From the laser spot size and the measured incident and reflected beam powers we determined an effective excitation power density of ~0.64 W/cm^2 in the spot at the exit face of the sample under test. This level of optical power density was sufficient for the generation of photoluminescence spectra from a variety of wafers with acceptable SNR's.

The photoluminescence light from the sample is collected by an achromatic objective lens ($L1$), and focused into

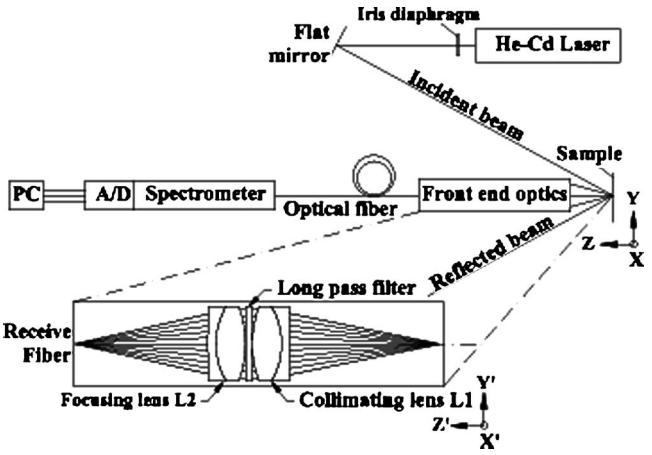

FIG. 1. Schematic diagram of the experimental setup and details of the front end optics.

the fiber optic patch by an achromatic lens ($L2$). The optical fiber is a multimode step index fiber (Ocean Optics model QP600-2-VIS-NIR). The multiline electronics interface from the spectrometer leads to an A/D converter card (Ocean Optics model ADC1000) connected to a Pentium PC. An Ocean Optics software is used to collect and process the data. Data correction and other post-treatment analysis were carried out in both MATLAB (MathWorks, Inc., Natick, MA) and ORIGINLAB (OriginLab Co., Northampton, MA).

While focusing, the laser incident beam on the sample increases the effective optical power density on the sample, the current design is not targeted to yield microspatial information about the origin of photoluminescence signals within the sample (hence the term macro-PL). Using matched illumination and collection optics with back focal plane apertures, enhanced spatial resolution, and improved depth profiling can be obtained using a confocal optical design which employs either local excitation or local detection of the PL signal or both.[1] Even higher resolutions can be achieved by use of solid immersion lenses (SILs).[21] Sophisticated microscope instruments based on this approach are commercially available. However, if the sample is heterogeneous on a size scale comparable to the laser focus, there may be significant variations in photoluminescence intensity, depending upon which sample part is observed. A focused laser will produce a photoluminescence spectrum which is heavily influenced by the composition of the microstructure at the focus, and repetitive testing of a given sample may yield considerable spectroscopic signal variations. If the laser spot is larger (as in this system), the photoluminescence spectrum represents a spatial average over the sampled area, which approaches the bulk composition of the sample. The image of the core of the receiving fiber on the exit surface of the sample is smaller than the laser spot size on the sample and is at its center. Thus, the variations in power density across the sampled area are negligible. A day-to-day monitoring of the laser power and the collection function of the instrument are accomplished by measuring the PL signature of a stable reference sample of known PL spectrum.

B. Front end optics

The front end optical design is largely determined by the receiving fiber characteristics. The factors, such as sample location and accessibility, are key to the design specifications. The major problems with utilizing tiny, short-focal-length lenses are the practical considerations of handling, mounting, and positioning them relative to the sample under test. Ideally a sample should be easily loaded, observed, well illuminated and it should return sufficient signal in the spectral region of interest to provide a high SNR with high spectral resolution.

The effective f numbers of the lenses used are determined by the required magnification and the need to match the NA of the optical fiber. The effective f number, $F/\#$, of a lens and numerical aperture (NA) are related by

$$F/\# = f/d = 1/(2\mathrm{NA}), \tag{3}$$

where d is the effective aperture diameter of the lens.

The numerical aperture of a fiber is fixed by the fiber characteristics and is defined by the index of refraction of its core and cladding, determines the maximum solid angle at which a beam can be launched into it. Using a $\sim$0.22 NA fiber, this acceptance angle is $\sim$25.4°. The fiber cable is a key specification for magnification M. The required magnification is given by the ratio of the focal lengths of the collimating (L_1) and focusing lenses (L_2). A combination of two achromatic lenses (f=50 mm, d_o=25.4 mm) that meets the design specification were chosen to give a magnification of $\sim$1. It is well known that in the presence of spherical aberration, the best focus is not at the paraxial focus. Introduction of a small focus shift for each lens was used to minimize the transverse ray aberration and increase fiber coupling efficiency. An adjustable focus assembly was used to determine the optimum separation between the image plane and the focusing lens. The diameter of each lens was reduced to an effective value to allow coupling the beam into the fiber at its full acceptance angle.

Achromatic doublets lenses were chosen for the front end optics due to their high image quality. The design of these doublets uses the helium D line (587.6 nm) and the hydrogen F (486.1 mm) and C (656.3 nm) lines. Such wavelengths reasonably represent the visible spectrum. The doublets are computer optimized to provide excellent performance in the visible region. When chromatic aberration must be controlled, a doublet is typically employed. Frequently, a diffraction limited spot may be achieved when using a monochromatic source.

In addition, since the laser light is much brighter than any PL signal, its harmonics might be detected at the output of the spectrometer. The current design allows for a long pass filter (Thorlabs-FGL400: 1 in. round colored glass filter, 400 nm long pass filter) to be placed between the two lenses of the collection optics to block the laser light from entering the spectrometer. This filter has been selected for its excellent cutoff characteristics at the laser wavelength while providing an economically priced solution.

C. Mechanical design

To minimize the position alignment error between the center of the illuminated sample and the optical axis of the collimating lens, the front end optics are placed in 1 in. internal diameter black anodized aluminum series lens tubes held by a multiaxis translation stage (X',Y',Z'), which provides a long-term positional stability (Fig. 1). The collection optics tube minimizes the position alignment error between the center of the receiving fiber and the optical axis of the focusing lens, and thus the angle alignment error caused by the tilt of the optical axis of the collimating lens with respect to that of the focusing lens. The optics are secured in the tubes by retaining rings placed at the desired locations inside the tube. A fiber connector adapter end plate is used to allow the receiving end of the fiber to be integrated into the series lens tubes. The other end of the fiber optic cable is connected to the spectrometer.

The movable sample holder slides into a fixture normally installed on a second translation stage (X,Y,Z). Adjustments of the two axes in the plane perpendicular to the optical axis of the front end optics allows the proper positioning of sample at the incident laser beam line, while the third axis (normally fixed for a given sample thickness) keeps the exit face of the illuminated sample at the proper distance from the collimating lens. This arrangement minimizes the alignment errors that will result in an error in the position of the image on the end face of the receiving lens, causing a position error between the image of the illuminated sample and the receiving fiber core, which will result in a loss of light in the coupling. Submicron incremental movements are readily achievable with this design.

IV. CALIBRATION

A. Spectral calibration

Wavelength calibration is fundamental to the provision of high-quality data. Regular calibration also provides a rigorous way of monitoring system performance over time. The relation between pixel position and measured wavelength was determined using the emission spectra of a pencil style mercury (argon) lamp [Oriel Hg (Ar)-6035]. This lamp is insensitive to temperature. It requires a 2 min warm up for the mercury vapor to dominate the discharge, then 30 min for complete stabilization. The average intensity is remarkably constant and reproducible after the thermal conditions stabilize. Regression analyses were used to correlate the pixel positions with the true wavelengths. A third order polynomial model was fitted:

$$\lambda_P = \lambda_0 + \sum_{i=1}^{3} c_i p^i, \tag{4}$$

where λ_P is predicted wavelength of pixel p, c_i is the ith coefficient, and λ_0 is the wavelength corresponding to the first pixel. The choice of the order of the polynomial depends on the nonlinear behavior of the spectrometer. The Ocean Optics software[20] allows the calibration parameters $(\lambda_0, C_1, C_2, C_3)$ to be stored in a configuration file.

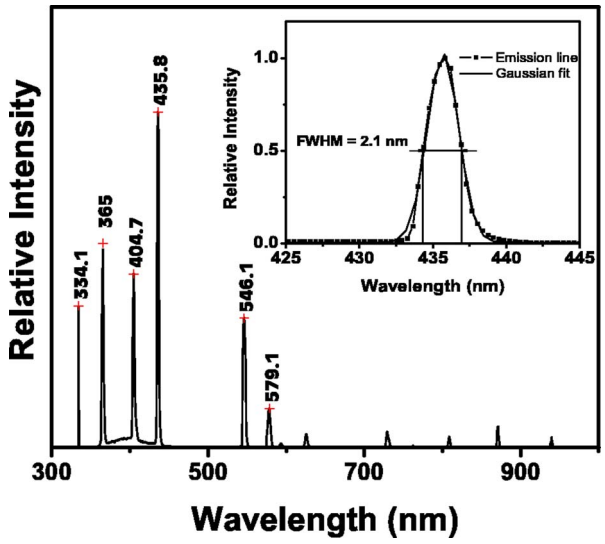

FIG. 2. Output spectrum of an Oriel 6035 Hg(Ar) lamp, run with an Oriel 6047 power supply. The spectra is measured with S2000 with 50 μm slit excluding the front end optics. The inset shows the emission peak at ~435.8 nm and its Gaussian fit. The FWHM of the Gaussian fit is 2.1 nm.

Figure 2 shows a few of the emission lines of an Oriel 6035 Hg(Ar) lamp, run with an Oriel 6047 power supply. The spectra are measured with S2000 with 50 μm slit excluding the front end optics. Note that the intensity of the other emission lines above 600 nm can become stronger by using higher integration times in the spectral measurement. The inset shows the emission peak at ~435.8 nm and its Gaussian fit. The FWHM of the Gaussian fit is 2.1 nm. Assuming that this emission line has an insignificant spectral spread, then the width of this emission line when measured represents the linewidth imposed by the instrument (instrumental function).

B. Instrument response function and intensity calibration

The instrument response function is the product of several instrumental variables that depend on the wavelength, including CCD response, transmissions of the optical fiber, lenses, and filter, in addition to the effects of the internal optics of the spectrometer such as grating reflectivity and optical alignment. Therefore a PL spectrum which is uncorrected for this instrumental response function is subject to distortion relative to the true spectrum, and may differ from laboratory to laboratory. The correction for instrument response necessitates either an accurate knowledge of the wavelength dependence of all components in the system, or a standard source with known spectral output. The former approach is difficult and by and large impractical. In this work the instrument response function is determined by measuring the output of a light source with known spectral distribution. The spectrometer is calibrated by measuring the output of a lamp of standard irradiance (Ocean Optics: LS-1-CAL) designed for optical fibers.[22] The lamp is NIST traceable and provides absolute spectral irradiance in μW cm^{-2} nm^{-1} at the receiving fiber port. The lamp's calibration file has only a limited number of data points over the 300–1050 nm range, so a MATLAB interpolation routine was used to find the spec-

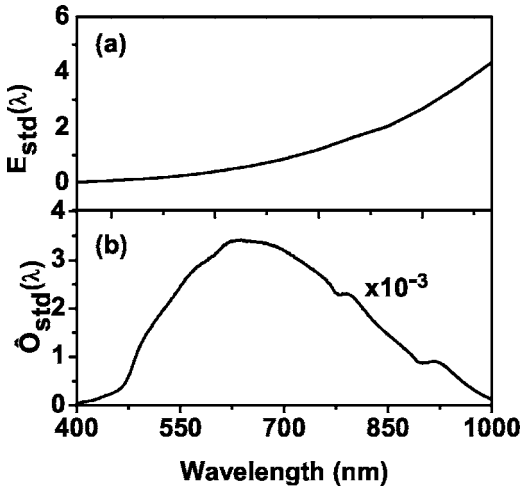

FIG. 3. (a) Output of the calibrated lamp in μW cm^{-2} nm^{-1}. (b) Measured dark current-subtracted scan of the calibrated light source (units in A/D counts) using an integration time of 40 ms. It is seen that the detector response peaks around 630 nm giving 3415 A/D counts and tapers off as one moves to blue or near infrared wavelengths.

tral irradiance values at the spectrometer wavelengths for the entire spectrometer range. Figure 3 shows the output of the calibrated lamp in μW cm^{-2} nm^{-1} and the corresponding measured dark current-subtracted scan of the calibrated light source (units in A/D counts) using an integration time of 40 ms.

It is seen that the detector response peaks around 630 nm giving 3415 A/D counts and tapers off as one moves to blue or near IR wavelengths.

The energy response function (μJ count^{-1}) (Fig. 4) for each pixel in the CCD, $R_J(\lambda)$, can be written as

$$R_J(\lambda) = E_{\text{std}}(\lambda)\Delta\tau_{\text{std}}A_{\text{fiber}}\Delta\lambda_{\text{pixel}}[\hat{O}_{\text{std}}(\lambda,\Delta\tau_{\text{std}})]^{-1}, \quad (5)$$

where $E_{\text{std}}(\lambda)$ is the standard spectral irradiance of the calibration lamp in μW cm^{-2} nm^{-1} at the receiving fiber port. $\Delta\tau_{\text{std}}$ is the CCD's integration period in seconds used in the measurement of the output of the calibrated lamp, A_{fiber} is the fiber's core area in cm^2, $\Delta\lambda_{\text{pixel}}$ is the CCD's pixel bandwidth in nanometers, and $\hat{O}_{\text{std}}(\lambda,\Delta\tau_{\text{std}}) = \bar{O}_{\text{std}}(\lambda,\Delta\tau_{\text{std}}) - \bar{O}_{\text{dark}}(\lambda,\Delta\tau_{\text{std}})$ is the measured or "observed" time-averaged and dark current-subtracted scans of the calibrated light source (units in A/D counts). This measurement is typically made using the bare fiber with the LS-1-CAL exclusive of the front end optics (the two lenses and the filter). With a specially designed connector barrel which can be screwed onto the end of the fiber, the barrel and the fiber are inserted completely into a factory-installed SMA connector of the LS-1-CAL.

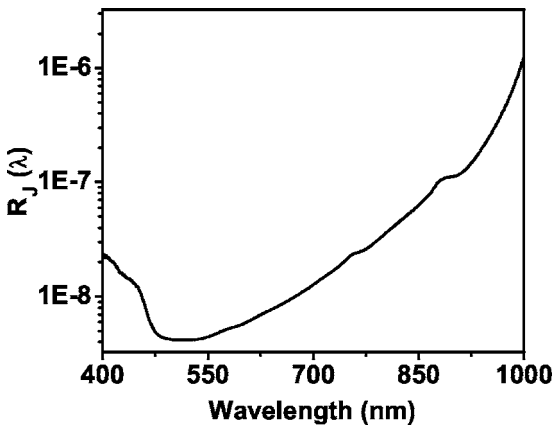

FIG. 4. Energy response data for each pixel in the CCD, for the spectral range 400–1000 nm.

The dark current scan is measured while the light path to the spectrometer is blocked (units in A/D counts) and $\Delta\tau_{\text{std}}$ is the integration period in seconds used in the measurement of both, $\bar{O}_{\text{std}}(\lambda,\Delta\tau_{\text{std}})$ and $\bar{O}_{\text{dark}}(\lambda,\Delta\tau_{\text{std}})$.

It can be shown that the observed signal (μW cm^{-2} nm^{-1}) representing the fraction of total photoluminescence flux of the sample, per unit area, that is detected by the spectrometer and corrected for the full instrument response function (which includes the transmission effects of the optical fiber, lenses, and filter, in addition to the effects of the internal optics of the spectrometer and the CCD response) is

$$\Delta\bar{E}_{\text{sample}}(\lambda) = \frac{C_F(\lambda)^{-1}\hat{O}_{\text{sample}}(\lambda,\Delta\tau_{\text{sample}})}{\hat{O}_{\text{std}}(\lambda,\Delta\tau_{\text{std}})}\left[\frac{\Delta\tau_{\text{std}}}{\Delta\tau_{\text{sample}}}\right]E_{\text{std}}(\lambda), \quad (6)$$

where $\hat{O}_{\text{sample}}(\lambda,\Delta\tau_{\text{sample}}) = \bar{O}_{\text{sample}}(\lambda,\Delta\tau_{\text{sample}}) - \bar{O}_{\text{dark}}(\lambda,\Delta\tau_{\text{sample}})$ is the measured time-averaged and dark current-subtracted PL spectrum of the sample, and $\Delta\tau_{\text{sample}}$ is the integration period in seconds used in these two measurements. $C_F(\lambda)$ is a wavelength dependent front end optics correction factor. This unitless factor accounts for the transmission losses in the front end optics and any fiber-coupling mismatch due to their use. Determination of $C_F(\lambda)$ requires two independent measurements. First, the calibrated lamp is placed as a source (simulating a sample under test) and a spectrum, $\hat{O}_{\text{feo}}(\lambda,\Delta\tau)$ is measured with the utilization of the front end optics. The second measurement $\hat{O}_{\text{dc}}(\lambda,\Delta\tau)$ is made for the same emission spectrum of the lamp but using direct coupling with the bare fiber exclusive of the front end optics. The ratio of the measurements gives

$$C_F(\lambda) = \hat{O}_{\text{feo}}(\lambda,\Delta\tau)/\hat{O}_{\text{dc}}(\lambda,\Delta\tau), \quad (7)$$

where $0 \leqslant C_F(\lambda_i) < 1$.

Figure 5 shows a typical measured correction function for the front end optics which included the two visible achromatic doublets and the long pass filter. The measured percentage transmittance of the long pass filter is also shown for comparison. The quality of $C_F(\lambda)$ above ~700 nm can be improved by using near IR achromatic doublets specially coated for optimal performance in the near IR range (e.g., at design wavelengths 706.5, 855.0, and 1015 nm).

The following conversion factor restates Eq. (6) in photons s^{-1} cm^{-2} nm^{-1},

$$\Delta E(\text{photons s}^{-1}\text{ cm}^{-2}\text{ nm}^{-1}) = \frac{\lambda}{hc}10^6\Delta E(\mu\text{W cm}^{-2}\text{ nm}^{-1}), \quad (8)$$

where h is Planck's constant and c is the speed of light.

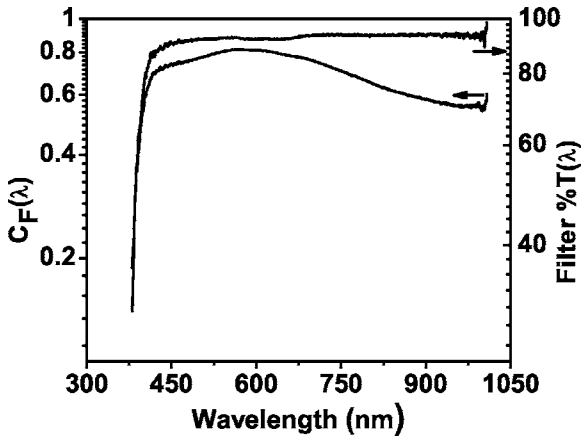

FIG. 5. A typical measured correction function for the front end optics which included the two achromatic doublets and the long pass filter. The measured percentage transmittance of the long pass filter is also shown for comparison.

V. APPLICATION TO SiO_x AND DISCUSSION

The performance tests of this PL system showed that the instrument would generate unambiguous spectra of luminescence in SiO_x ($x \leqslant 2$) wafers. Silicon nanocrystal formation in the silicon rich silicon oxide thin films has been described in detail elsewhere.[23] Here, only a practical demonstration of the utility of this PL system is given. Figure 6 demonstrates the effect of silicon content upon the PL spectra of two samples produced using an Electron Cyclotron Resonance Plasma-Enhanced Chemical Vapor Deposition (ECR-PECVD) system, the details of which are described elsewhere.[24] The films are each 100 nm thick, deposited on silicon substrates and were annealed at temperatures of 1100 °C for 2 h under argon to precipitate the nanocrystals. The inset shows the image of red photoluminescence from the SiO_x film using the UV (325 nm) He–Cd laser pump. The spectra are corrected according to Eq. (8) followed by peak normalization to show the relative PL peak intensities. As can be seen in the figure the emission shifts to longer wavelengths as the silicon content increases. This is presumably because the increased silicon content leads to larger nanocrystals and this in turn, leads to a redshifting of the photoluminescence, which is consistent with the quantum confinement model.[25]

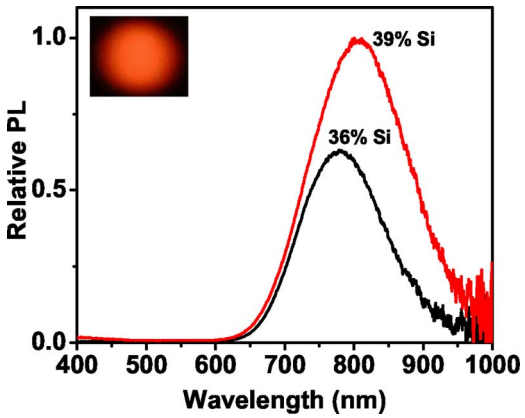

FIG. 6. Corrected PL spectra of nc-Si for two Si concentrations. The inset shows the image of red photoluminescence of a SiO_x film (39% Si) using a UV (325 nm) He–Cd laser pump. The noise above ~850 nm is due to combined effects of low signal level and the reduced sensitivity of the CCD in this region.

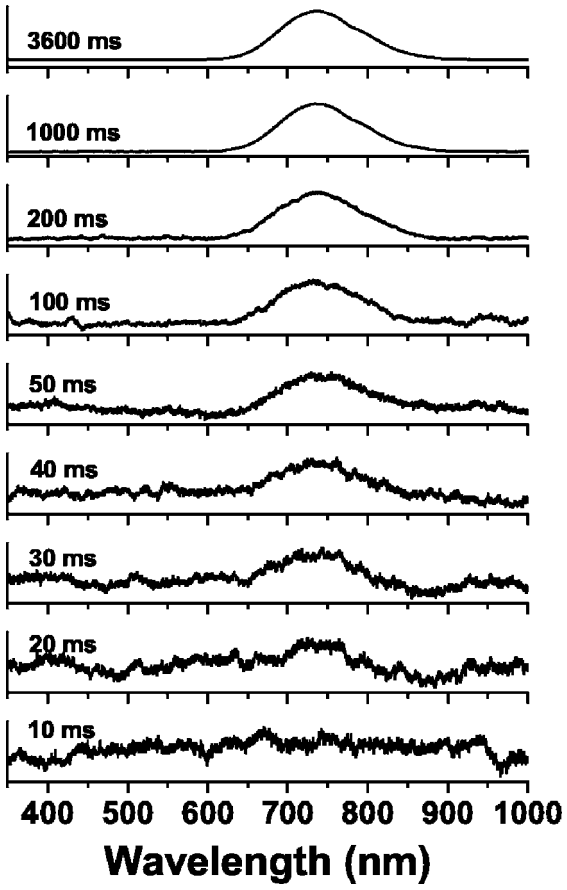

FIG. 7. Measured dark current-subtracted PL spectra of silicon rich silicon oxide sample (units in A/D counts) using various integration times ranging from 10 to 3600 ms with no averaging and no boxcar smoothing. The sample has a refractive index of the active film layer of ~1.5 and was annealed at 1100 °C for 30 min in a nitrogen ambient. Increasing the integration time boosts the signal (scale not shown) and improves SNR.

The noise above ~850 nm is due to the combined effects of low signal level and the reduced sensitivity of the CCD in this region. In acquiring the raw data of these spectra, we used an integration time of 2500 ms for each spectrum, and averaged ten spectra using a smoothing size of $n_b=2$. With the current A/D converter the acquisition software allows integration times from 3 ms up to 60 s. Thus with the background subtraction a much improved SNR over the entire spectral range can be achieved using higher integration times, and/or larger number of averages. Obviously, increasing the integration time in order to improve the SNR is valid only till saturation.

To demonstrate the significance of the integration time function on the quality of the spectra in this application and to highlight the distinct benefit of this approach over the single element detection (which has no integration function) we present Fig. 7 which shows the measured dark current-subtracted PL spectra (units in A/D counts) of a SiO_x ($x < 2$) sample, using various integration times ranging from 10 to 3600 ms with no averaging and no boxcar smoothing. The sample has a refractive index of the active film layer of

~1.5 and was annealed at 1100 °C for 30 min in a nitrogen ambient. It is clear that increasing the integration time boosts the signal (scale not shown) and improves SNR. The spectrum with the highest integration time is near saturation and has SNR of ~250:1. At this level further enhancement of SNR is possible using averaging and background subtraction as described above. For this application, the results demonstrate that the present signal to noise enhancement technique can be a viable low cost alternative to CCD cooling where the signal level is invariant over long periods (limited by some practical observation time).

The spectrometer employed in the present prototype features a miniature optical design configured for an optical bench small enough to fit into the palm of your hand. The footprint of the spectrometer package is $\sim 15 \times 15$ cm^2, but the actual spectrometer part of the pack is small. Despite its tiny size, the results demonstrate that good quality PL data comparable to those normally generated from larger conventional monochromators with moderate performance can be delivered. The stray light is less than 0.05% at 600 nm (manufacturer specified). The grating is static, i.e., the spectrometer has no moving parts associated with the wavelength scale. This result in a very stable optical system and reproducible wavelength accuracy. One key advantage here is that averaging may be executed easily, and without the risk of signal degradation caused by nonreproducibility of the scanning system. Older systems based on mechanical scanning often involved mechanical clutches and linkages between monochromators, and the monochromator drives were cam driven. This often resulted in problems associated with backlash and hysteresis within the drive mechanisms generating the potential for wavelength scale error from scan to scan. However, more modern instruments feature direct drive monochromators where the grating is mounted on a shaft of a digitally controlled stepper motor. This removes most of error sources described.[26] Thus with a fixed grating spectrometer with CCD array detection, one clearly overcomes most of the original disadvantages cited for dispersive instruments based on the mechanical scanning. The additional evident advantage of this technique over a single element detection is the ability to perform simultaneous multiwavelength measurements which reduces the spectral acquisition time significantly compared with a scanning monochromator having the same spectral resolution, and hence the speed advantage.

The spectrometer used in the present application is sensitive enough to record the weak-emission based PL spectra of nanocrystalline silicon materials, rare-earth dopants, and silicon rich silicon oxide, SRSO, films in less than few seconds and yet still retails for the remarkably low price and for a fraction of the cost of larger systems.

Optical multichannel analyzers (OMA's) have also been used in the photoluminescence experiments.[27–30] The detector typically an image-intensified PDA is mounted directly in the focal plane of a monochromator and controlled by an OMA.[27] The monochromator or spectrometer comes usually with footprints of few square feet in size depending on the focal length. Double- and triple-monochromator systems are also commercially available, however, while these provide the desired optical properties, the very large footprint and cost of these systems, often places them beyond the reach of many laboratories.

The intensified detector possesses high sensitivity and greater ability to time resolve. The fast OMA's are generally convenient for nonrepetitive signals, and for generating time-series spectrum data.[31–33] Apart from the excitation source, the quality and size of the imaging area of the detector and associated electronics tend to dictate the total price. This is exemplified in the newest OMA V detectors from Princeton Instruments/Acton that utilize linear PDAs designed to offer excellent near IR sensitivity from 1.0 to 2.2 μm. Likewise, for the visible and near IR applications, high performance intensified charge-coupled device (ICCD) camera systems are available. For example, the PI-MAX camera head: 1024 (1024×256 imaging array) from Princeton Instruments/Acton has subnanosecond gating capability and an integrated programmable timing generator that make these ICCD cameras distinguished for time-resolved applications.

VI. SUMMARY

We have carefully characterized and described the various design requirements and calibration for a low cost laser macro-PL system for silicon-based photonics based on CCD detection. The mechanical and optical designs are also presented. No expensive and sophisticated components are required. The system has been shown to acquire accurate PL data with acceptable spectral resolution and satisfactory SNR within the measurement times of few seconds for a relatively wide spectral window. The results demonstrate that the present signal to noise enhancement technique can be a viable low cost alternative to CCD cooling in steady state photoluminescence experiments where the signal level is invariant over long periods (limited by some practical observation time). The method employed has resulted in a versatile system whilst retaining the convenience associated with a computer-controlled system.

We have highlighted the importance of correction for instrument response function and optics transmission which is often overlooked. This work is also important in evaluating the techniques available, so that the optimal choice, in terms of speed, cost, or sensitivity, may be selected, and to evidence the peculiarities of this technique and to allow its use at the best of its capabilities.

This system is now being used at our institution in several applications including process control and evaluation of new materials and research efforts to determine optimum film composition and post-treatment parameters to yield good devices.

ACKNOWLEDGMENTS

This work is supported by the Natural Sciences and Engineering Research Council of Canada, Ontario Centers of Excellence Inc., Photonics Research Ontario, and the Ontario Research and Development Challenge Fund under the Ontario Photonics Consortium. Dr. Doug M. Bruce is acknowledged for valuable technical input.

[1] T. H. Gfroerer, in *Encyclopedia of Analytical Chemistry*, edited by R. A. Meyers (Wiley, Chichester, 2000), pp. 9209.
[2] V. Vinciguerra, G. Franzo, F. Priolo, F. Iacona, and C. Spinella, J. Appl. Phys. **87**, 8165 (2000).
[3] K. Watanabe, H. Tamaoka, M. Fujii, and S. Hayashi, J. Appl. Phys. **92**, 4001 (2002).
[4] B. G. Fernandez, M. Lopez, C. Garcia, A. Perez-Rodriguez, J. R. Moerante, C. Bonafos, M. Carrada, and A. Claverie, J. Appl. Phys. **91**, 798 (2002).
[5] N. A. Sobolev, O. B. Gusev, E. I. Shek, Vl. Vdovin, T. G. Yugova, and A. M. Emel'yanov, Appl. Phys. Lett. **72**, 3326 (1998).
[6] E. Degoli, S. Ossicini, D. Barbato, M. Luppi, and E. Pettenati, Mater. Sci. Eng., B **69–70**, 444 (2000).
[7] I. Umezu, G. Yamazaki, T. Yamaguchi, A. Sugimura, T. Makino, Y. Yamada, N. Suzuki, and T. Yoshida, Mater. Sci. Eng., C **15**, 129 (2001).
[8] Y. C. Fang, W. Q. Li, L. J. Qi, L. Y. Li, Y. Y. Zhao, Z. J. Zhang, and M. Lu, Nanotechnology **15**, 494 (2004).
[9] A. Malinin, S. Novikov, V. Ovchinnikov, V. Sokolov, O. Kilpelä, T. Saloniemi, and J. Sinkkonen, Reports in Electron Physics 2001/25, Espoo 2001, ISBN 951-22-5428-X, Helsinki University of Technology 2001.
[10] M. Fujii, M. Yoshida, S. Hayashi, and K. Yamamoto, J. Appl. Phys. **84**, 4525 (1998).
[11] F. Iacona, G. Franzo, and C. Spinella, J. Appl. Phys. **87**, 1295 (2000).
[12] J. W. Olesik and J. P. Walters, Appl. Spectrosc. **38**, 578 (1984).
[13] T. Vo-Dinh and D. Eastwood, *Laser Techniques in Luminescence Spectroscopy* (ASTM International, Philadelphia, 1990), pp. 175.
[14] A. Harmer and G. E. Boisde, *Chemical and Biochemical Sensing With Optical Fibers and Waveguides* (Artech, Boston, 1996).
[15] A. Bignazzi, E. Grilli, M. Radice, M. Guzzi, and E. Castiglioni, Rev. Sci. Instrum. **67**, 666 (1996).
[16] *Diffraction Grating Handbook*, 6th ed., edited by C. Palmer (Newport Corporation, New York, 2005).
[17] W. H. Steel, Appl. Opt. **13**, 704 (1974).
[18] J. D. E. Beynon and D. R. Lamb, *Charge Coupled Devices and Their Applications* (McGraw-Hill, London, 1980).
[19] H. J. Larson, *Introduction to Probability Theory and Statistical Inference* (Wiley, New York, 1982).
[20] *Operating Manual and User's Guide: S2000 Fiber Optic Spectrometer* (Ocean Optics, Dunedin, FL, 2004).
[21] S. Moehl, H. Zhao, B. D. Don, S. Wachter, and H. Kalt, J. Appl. Phys. **93**, 6255 (2003).
[22] *Ocean Optics-Light Catalog* (Ocean Optics, Dunedin, FL, 2004).
[23] T. R. Roschuk, J. Wojcik, E. A. Irving, M. Flynn, and P. Mascher, Proc. SPIE **5577**, 450 (2004).
[24] M. Boudreau, M. Boumerzoug, P. Mascher, and P. Jessop, Appl. Phys. Lett. **63**, 3014 (1993).
[25] G. Ledoux, J. Gong, F. Huisken, O. Guillois, and C. Reynaud, Appl. Phys. Lett. **80**, 4834 (2002).
[26] J. Cazes, *Ewing's Analytical Instrumentation Handbook*, 3rd ed., edited by J. Cazes (Marcel Dekker, New York, 2005), pp. 1037.
[27] S. Mochizuki, F. Fujishiro, and S. Minami, J. Phys.: Condens. Matter **17**, 923 (2005).
[28] C. Courteille, J. L. Dorier, J. Dutta, C. Hollenstein, A. A. Howling, and T. Stoto, J. Appl. Phys. **78**, 61 (1995).
[29] J. Dutta, I. M. Reaney, P. R. I. Cabarrocas, and H. Hofmann, Nanostruct. Mater. **6**, 843 (1995).
[30] V. Pellegrini, F. Fuso, G. Lorenzi, M. Allegrini, A. Diligenti, A. Nannini, and G. Pennelli, Appl. Phys. Lett. **67**, 1084 (1995).
[31] G. F. Albrecht, E. Kallne, and J. Meyer, Rev. Sci. Instrum. **49**, 1637 (1978).
[32] G. Chini, K. Kelbert, and H. Bettermann, Rev. Sci. Instrum. **62**, 1234 (1991).
[33] J. A. Antoniades and T. Peyser, Rev. Sci. Instrum. **58**, 253 (1987).